

# Wake Vortex Detection and Tracking for Aircraft Formation Flight

Denis-Gabriel Caprace\*, Grégoire Winckelmans†, Philippe Chatelain‡  
*Institute of Mechanics, Materials and Civil Engineering*  
*Université catholique de Louvain, 1348, Louvain-la-Neuve, Belgium*

Jeff D. Eldredge§  
*Mechanical and Aerospace Engineering Department*  
*University of California, Los Angeles, Los Angeles, CA, 90095, USA*

Formation flying is known to improve the aerodynamic efficiency of a follower aircraft flying close to the wake vortices of a leader. In this study, two wake sensing strategies designed to locate these vortices are exposed. The first one is based on dedicated measurements of the follower wing circulation distribution and on the control surfaces deflections. The second one relies on measurements from its flight dynamics (position, velocity) and control surfaces. Both techniques implement an Ensemble Kalman Filter for the propagation in time of the non-linear surrogate model, which involves Prandtl lifting lines for the aerodynamics, and a simplified equation of motion. The resulting estimators are tested under steady and unsteady flight conditions, using reference data obtained from the numerical simulation of the associated wake flows using CFD. As a result, an accurate estimation of the wake parameters is produced by both methods, even in configurations where a symmetry was known to hamper the filter efficiency. Noisy configurations are also considered through the addition of ambient turbulence in the simulations. In that case, the second method proves more sensitive to external perturbations.

## Nomenclature

|                      |   |  |
|----------------------|---|--|
| $\alpha_g$           | = | geometric angle of attack                            |
| $A_R$                | = | aspect ratio   |
| $b$                  | = | wing span  |
| $C_L$                | = | lift coefficient                                     |
| $C_l$                | = | rolling moment coefficient                           |
| $C_n$                | = | yawing moment coefficient                            |
| $\Delta y, \Delta z$ | = | follower aircraft relative position to leader's wake |
| $\mathbf{f}$         | = | process function                                     |
| $\Gamma$             | = | circulation  |
| $\mathbf{h}$         | = | measurement function                                 |
| $\mathbf{H}$         | = | measurement matrix                                   |
| $h$                  | = | numerical mesh resolution                            |
| $\mathbf{K}$         | = | Kalman gain  |
| $\mathbf{m}$         | = | estimated measurement vector                         |
| $N$                  | = | ensemble size  |
| $\mathbf{P}$         | = | state covariance matrix                              |
| $\mathbf{q}$         | = | state vector   |
| $\rho$               | = | air density  |
| $S$                  | = | reference surface                                    |
| $U_\infty$           | = | upstream velocity                                    |

---

\*F.R.S.–FNRS Research aspirant fellow; denis-gabriel.caprace@uclouvain.be.

†Full professor; gregoire.winckelmans@uclouvain.be. Senior Member AIAA.

‡Professor; philippe.chatelain@uclouvain.be.

§Professor; eldredge@seas.ucla.edu. Associate Fellow AIAA.

$\mathbf{V}$  = measurement noise covariance matrix  
 $x_f, y_f, z_f$  = follower aircraft position  
 $\mathbf{y}$  = innovation  
 $\mathbf{z}$  = actual system measurement vector

## I. Introduction

Formation flying is a bio-inspired technique and has long been known for its aerodynamic benefits. Early investigations conducted on a pair of aircraft (leader + follower) indeed showed that a substantial drag reduction can be achieved by the follower, both theoretically [1] and experimentally [2, 3]. Therefore, large fuel savings are at stake when it comes to the integration of formation flight into commercial aviation. This explains why the topic is still intensively researched today (e.g. [4, 5]).

While birds usually fly in close formation, extended formation flight seems more attractive in the context of civil aviation, for obvious safety reasons. In that case, the follower is flying at several tens of wingspans downstream of the leader. Because wake vortices are strong, long-lasting flow structures, the follower still benefits from a positive interaction with the leader's wake vortices [6, 7]. However, in such a configuration, it becomes important to precisely maintain the relative position between the follower aircraft and the leader's wake vortices, as the drag reduction achieved is very sensitive to that positioning (instead of aircraft relative positioning). Additionally, because of the longer distance between the leader and the follower, instabilities such as meandering [8] and external factors [9] may affect the motion of the vortices. It is therefore essential for the follower to continuously locate the wake vortices. This information can then be provided to an autopilot, which will maintain the aircraft at the optimal location and therefore keep the savings at their best during the flight.

Several methods allowing the follower to track the vortices have been proposed, yet little documentation is available about their implementation in actual formation flight experiments. The position and strength of the vortices can be determined from a direct measurement of the flow field [10, 11], e.g. through a LIDAR installed on the aircraft. Today, even though ground based measurements provide sufficiently reliable results [12], the use of such technologies still poses significant challenges for on-board wake measurements [13].

Alternatively, a vortex sensing technique has been proposed to estimate the wake vortex parameters [14]. It uses distributed pressure measurements on the follower wing which are processed by an estimator, essentially based on an Extended Kalman Filter (EKF), to deduce the parameters of the wake vortices currently influencing the follower. This technique showed promising results in several flight configurations, especially for deducing the position of the vortices, even though some observability issues were highlighted [15].

The present study is intended to enhance the vortex sensing technique by exploring new strategies based on different sets of measurements, as well as by improving the estimator itself. The latter uses a state model of the process based on a Prandtl lifting line model that crudely characterizes the aerodynamics of the follower. It also captures the influence of the leader's wake vortices. Additionally, some ingredients were added in order to make it usable in unsteady configurations. Here, the estimators make use of an Ensemble Kalman Filter (EnKF), better suited to handle the non-linearity of the process [16] than the EKF.

Two distinct estimation strategies are established.

- 1) The first one is based on spanwise distributed circulation measurements (essentially equivalent to pressure measurements). Inputs from the aircraft attitude and yawing moment are also added, and their influence in the quality of the estimation of the wake vortices parameters is characterized. Notice that the use of dedicated sensors aboard the follower aircraft (e.g. pressure taps for the circulation measurement) would impose design constraints on the wing, and comes at an extra cost.
- 2) The second one does not rely on circulation measurements; inputs from the flight dynamics and flight controls are used as measurements instead, and the estimator is adapted accordingly. While more challenging, the estimation is here performed only using sensors already present on board today's commercial aircraft.

These techniques are tested in three flight conditions, respectively involving steady wakes, unsteady wakes and wakes with ambient turbulence. For each of them, 'truth' measurements are extracted from numerical simulations and serve as a reference for the estimators. Indeed, large eddy simulation is employed in order to obtain high-fidelity results of two aircraft flying in formation. The space-developing simulations involved capture the production of the wake vortices originating from the leader, their roll-up and the interaction with the follower's wake, optionally with inflow turbulence.

In this article, the method is first presented, including the estimator and the surrogate state model characterizing the process. Then the high-fidelity simulations representing various configurations of a two-ship formation flight are

introduced. Finally, the results of the filters are shown for the three flight conditions simulated, focussing on the accuracy of the estimated wake vortex parameters, for the two considered strategies.

## II. Estimator and Kalman filtering

This work relies on the discrete time Kalman filter framework to estimate the characteristics of the leader's wake vortices. Due to the relatively strong non-linearity of the system under investigation, the classical Kalman Filter (KF) cannot be used. The Extended Kalman Filter (EKF), which requires the linearization of the system about the current state, was also proven unsuccessful in some configurations when applied to the current problem [14]. Biases on the solution, or even diverging behaviors were observed, and are likely to be related to the observability structure of the wake, or to the non-linearity, causing an unstable growth of the error covariance.

To overcome these issues, the Ensemble Kalman Filter (EnKF) initially proposed in [17] is here employed. It uses a Monte Carlo approach to describe the probability density function of the states, meaning that the state vector  $\mathbf{q}$  is actually discretized using an ensemble of  $N$  members. The ensemble undergoes the propagation step, the analysis step, and the covariance inflation at every iteration of the filter.

The propagation step consists in evaluating

$$\mathbf{q}_i^{n+1|n} = \mathbf{f}(\mathbf{q}_i^n), \quad (1)$$

$$\mathbf{m}_i^{n+1|n} = \mathbf{h}(\mathbf{q}_i^{n+1|n}), \quad (2)$$

where  $\mathbf{q}_i^n$  is the  $i^{\text{th}}$  ensemble member state vector at iteration  $n$ ,  $\mathbf{m}$  is the measurement vector, and  $\mathbf{f}$  and  $\mathbf{h}$  are functions describing the process and the measurements (see section IV). The approximate mean and covariance matrix of the propagated state vectors  $\mathbf{q}_i^{n+1|n}$  are computed from the ensemble, respectively as

$$\hat{\mathbf{q}}^{n+1|n} = \frac{1}{N} \sum_{i=1}^N \mathbf{q}_i^{n+1|n},$$

$$\mathbf{P}^{n+1|n} = \frac{1}{N-1} \sum_{i=1}^N \left( \mathbf{q}_i^{n+1|n} - \hat{\mathbf{q}}^{n+1|n} \right) \left( \mathbf{q}_i^{n+1|n} - \hat{\mathbf{q}}^{n+1|n} \right)^T.$$

In the analysis step, the measurements taken from the “truth” (i.e. the actual system, see section III),  $\mathbf{z}^{n+1}$ , are compared to  $\mathbf{m}_i^{n+1|n}$  in order to produce the innovation

$$\mathbf{y}_i^{n+1} = \mathbf{z}^{n+1} - \mathbf{m}_i^{n+1|n} + \boldsymbol{\epsilon}_i^{n+1}, \quad (3)$$

where the random vector  $\boldsymbol{\epsilon}_i^{n+1} \sim \mathcal{N}(0, \mathbf{V}^{n+1})$  ensures the absence of spurious correlation in the ensemble covariance, with  $\mathbf{V}$  the measurement noise covariance matrix.

Then, the Kalman gain  $\mathbf{K}$  is used in its classical form to update the states:

$$\mathbf{K}^{n+1} = \mathbf{P}^{n+1|n} (\mathbf{H}^{n+1})^T \left( \mathbf{V}^{n+1} + \mathbf{H}^{n+1} \mathbf{P}^{n+1|n} (\mathbf{H}^{n+1})^T \right)^{-1}, \quad (4)$$

$$\mathbf{q}_i^{n+1} = \mathbf{q}_i^{n+1|n} + \mathbf{K}^{n+1} \mathbf{y}_i^{n+1}. \quad (5)$$

The measurement matrix  $\mathbf{H}$  is obtained in the frame of an “implicit linearized formulation” (as formulated in [18]). In practice, it means the state vector is extended with the measurements  $\mathbf{m}$  so that the non-linearity of  $\mathbf{h}$  is transferred to Eq. (1), while  $\mathbf{H}$  becomes linear. This procedure is also implemented in [19].

At this point, the covariance of the states is not bounded from below (as it is for the classical KF). As a last step, covariance inflation is thus implemented in order to prevent a covariance collapse which would render the filter inefficient. The state vector of each ensemble member is slightly altered by adding a small additive inflation  $\boldsymbol{\alpha}_i$ , i.e. a vector of random number following a Gaussian distribution with zero mean and with a covariance matrix corresponding to the process noise. The Relaxation To Prior Spread (RTPS) technique [20] is also used, finally leading to

$$\mathbf{q}_i^{n+1} \leftarrow \hat{\mathbf{q}}^{n+1} + \beta_i \left( \mathbf{q}_i^{n+1} - \hat{\mathbf{q}}^{n+1} \right) + \boldsymbol{\alpha}_i^{n+1}, \quad (6)$$

with  $\beta_i = 1 + \theta \left( \frac{\sigma_i^b - \sigma_i^a}{\sigma_i^a} \right)$ , where  $\sigma_i^a$  and  $\sigma_i^b$  are respectively the standard deviations of the prior (i.e.  $\mathbf{q}_i^{n+1|n}$ ) and of the posterior (i.e.  $\mathbf{q}_i^{n+1}$ ) states, and  $\theta = 0.7$ .

More details on the EnKF can be found in [21]. In addition to its ease of implementation, this approach enables the filtering of systems with a very large number of degrees of freedom for an affordable computational cost.

Notice that, as the number of degrees of freedom involved in the system considered here is small, the Unscented Kalman Filter (UKF) [22] would be a valid alternative to the EnKF. The UKF makes use of the unscented transform which propagates the statistics of the PDF through the non-linear system while ensuring that the mean and covariance of the propagated distribution are accurate up to the second order.

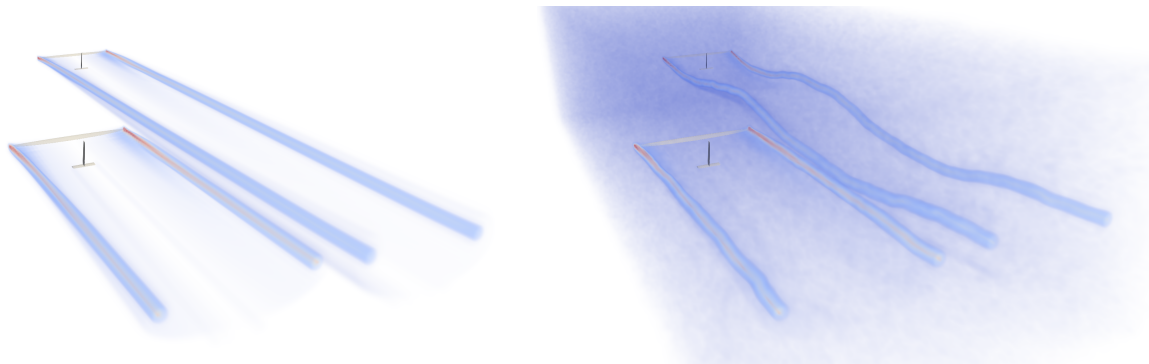
In this work, both the UKF and the EnKF were tested. As the obtained results were quite similar for a wide range of configurations, it was chosen to present only results obtained using the EnKF.

### III. Reference measurements and actual system representation

For the development of the current wake sensing approach, a realistic representation of the wake is needed in order to produce quality reference measurements which will be treated as the ‘truth’ in the estimator. To this end, the Vortex Particle-Mesh method (VPM) [23] is employed to simulate the eventually unsteady wake developed by a system of two aircraft in formation. The VPM method exploits the vorticity-velocity formulation of the Navier-Stokes equations expressed in a hybrid Lagrangian-Eulerian framework [24] in order to solve for unbounded incompressible flows. This large eddy simulation approach has been proven very efficient for the simulation of complex wake flows such as wind turbine wakes [25, 26] and helicopter wakes [27].

For the current application, the leader and the follower aircraft are identical and are represented through a set of three straight Immersed Lifting Lines (see Fig. 1): one for the wing (of span  $b$ ) with an elliptical chord distribution, one for the horizontal tail plane (HTP, of span  $b_h$ ) and one for the vertical tail plane (VTP, of span  $b_v$ ), both with constant chords. Each lifting line uses the local flow velocity and tabulated airfoil data to determine the vorticity that must be shed in the wake as a signature of lift. The vorticity is then advected with the flow, eventually undergoing strong interactions. The ensuing wake roll-up process is accurately captured, even at moderate to high Reynolds numbers, as the dissipation of the method is well controlled thanks to its Lagrangian character and the use of a Regularized Variational sub-grid scale Model [28].

The kinematics of the leader are prescribed, while the motion of the follower can be either prescribed or computed. Notice that the incidence of the HTP of both aircraft is set so as to cancel the pitching moment in isolated trimmed flight conditions.



(a) Simulation of a steady configuration without inflow turbulence      (b) Simulation with heaving motion of the leader and inflow turbulence

**Figure 1 Magnitude of the vorticity in the wake of two aircraft in formation flight**

In this work, the effect of inflow turbulence will be investigated as a natural source of process noise in the estimation routine. When activated, synthetic turbulence, generated using the Mann algorithm [29], is smoothly injected at the inlet of the computational domain (see Fig. 1b). This affects the wake generation mechanism and likely triggers vortex instabilities. As a result, the leader’s vortices have become unsteady by the time they reach the vicinity of the follower.

The reference parameters of the VPM simulations used to produce data for the estimator are reported in Table 1.

|                       |  |
|-----------------------|--|
| domain size           | $L_x \times L_y \times L_z = 8b \times 3b \times 2b$ |
| resolution            | $h/b = 1/64$   |
| HTP span              | $b_h/b = 0.2$  |
| VTP span              | $b_v/b = 0.25$                                       |
| wing aspect ratio     | $A_R = 20$   |
| HTP aspect ratio      | $A_{R,h} = 4$  |
| VTP aspect ratio      | $A_{R,v} = 3.25$                                     |
| main wing lift factor | $C_{L,w}/A_R = 0.1$                                  |

**Table 1** Parameters used in the VPM simulations

For all these numerical experiments, a longitudinal distance of  $4b$  was imposed between the leader and the follower. Incidentally, these conditions are not compliant with the hypothesis of extended formation flight, even though the roll-up process is here virtually accelerated by the use of a  $C_{L,w}/A_R$  about four times larger than that of cruising aircraft. The state of the wake at the location of the follower is thus roughly similar to that located at  $4 \times (4b)$  behind a cruising aircraft. Although this study aims at developing a tool suitable for extended formation flight, the choice of a small to moderate longitudinal separation distance was made to keep a relatively small time-to-solution for the simulations. All the present simulations were run on 48 CPUs for a maximum of 4 hours. Moreover, the fact that the vortices are not fully rolled-up can be seen as a source of process noise which the estimators are designed to be robust to. Therefore, the developed tools could be used for extended formation flight without restriction or adaptation, and the authors believe that the performance of the estimator would be similar.

The reference measurements needed for the estimator are taken from the simulations at every time step, which here also corresponds to the period of the filter  $T_f = dt$ . The follower circulation distribution is directly available through the use of the immersed lifting lines: the spanwise distributed measurement consists in the sampling of that distribution at 9 locations uniformly distributed across the wing. These quantities can be related to pressure measurements on the airfoil, as proposed in [14, 15]. Rolling and yawing moments are also computed from the outputs of the Immersed Lifting Line. Depending on the strategy, the kinematic variables of the follower (position, velocity) can also be passed to the EnKF.

## IV. Surrogate model

A state model representation is adopted for the system, as formally described by  $\mathbf{f}$  and  $\mathbf{h}$  in Section II. The model will be evaluated at every iteration of the EnKF filter, on each member of the ensemble. It is thus crucial for this surrogate model to be sufficiently faithful to reality while not too computationally expensive.

Two different models are now presented, which will enable two different estimation strategies.

### A. Aerodynamics model (Strategy 1)

The Prandtl Lifting Line (PLL) theory is used as the background aerodynamic model for the problem. It was elected for its relatively high degree of fidelity while remaining computationally affordable.

As depicted in Fig. 2, the follower aircraft is located at  $(0, y_f, z_f)$  and comprises a straight horizontal lifting line of span  $b$  for the wing and a vertical lifting line of span  $b_v$  for the VTP. There is no HTP in this model. The tail is located downstream of the wing at a distance  $d_v$  from the center of the wing (the same as in the CFD configuration). The geometric angle of attack (AoA) of the follower is  $\alpha_g$ , and is actually equal to the pitch angle of the plane. The wakes of the follower's wing and VTP are made of two flat vortex sheets going straight to infinity.

The wake of the leader is modeled as two counter-rotating vortex tubes of circulation  $\Gamma_0$  and spacing  $b_0$ . The vortices are aligned with the  $x$  axis, and are regularized using the high-order algebraic regularization, with a smoothing parameter of  $\sigma/b = 0.05$ . The center of the wake model in the plane  $(y, z)$  is located at a distance  $(\Delta y, \Delta z)$  from the position of the follower  $(y_f, z_f)$ .

With the PLL theory, one obtains an integro-differential equation which relates the circulation distribution of the wing and the VTP to the velocity induced on these lines by the leader's wake, and by their respective wake. The full set of equations to be solved can be found in [30], together with the method to solve them using spatial discretisation and sine series decomposition. The solution is the circulation distribution of the follower wing  $\Gamma(y)$ , and of the VTP  $\Gamma_v(z)$ .

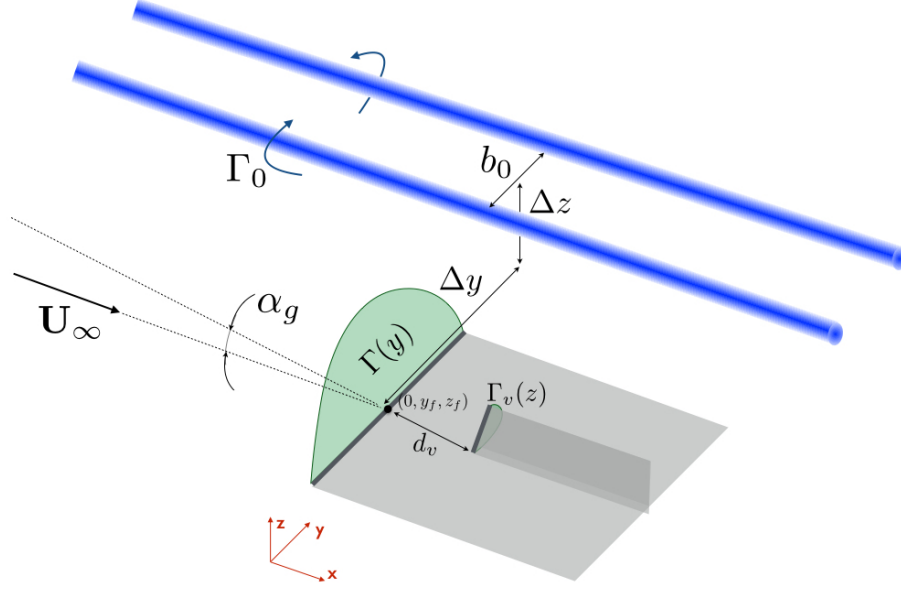


**Figure 2** Aerodynamic model of the follower with two lifting lines for the wing and the VTP and their respective wake (in gray), the leader's wake vortices (in blue) and the circulation distributions (in green).

The lift and drag forces are deduced from these distributions. The total aircraft yawing moment coefficient  $C_n$  and rolling moment coefficient  $C_l$  can then also be computed, both with contributions from the wing and the VTP. Notice that, from the yawing and rolling moments, one could evaluate the deflection angles of the control surfaces so as to obtain trim, which could be used as additional measurements. Since the follower is here frozen in roll and yaw, this is equivalent to using the moments themselves as measurements (assuming that there is no delay in the actuation of the control surfaces).

In summary, for the first estimation strategy based on aerodynamics only, the state variables are

$$\mathbf{q}_{\text{aero}} = [\alpha_g, \Gamma_0, \Delta y, \Delta z]^T,$$

and the other parameters ( $b_0, d_v, U_\infty$ ) are assumed constant. The list of available measurements is

$$\mathbf{m}_{\text{aero}} = [\alpha_g, \Gamma(y_1), \dots, \Gamma(y_k), C_n, C_l]^T$$

## B. Flight Dynamics model (Strategy 2)

The above aerodynamics model is complemented with a model for the flight mechanics. The latter makes use of the forces and moments computed by the aerodynamics model and integrates the aircraft equation of motion over time. This allows the prediction of the position, attitude and velocity of the follower over one iteration of the filter (i.e. one time step of the simulation).

Ideally, the follower equations of motion should obey the complete flight dynamics laws of the vehicle. However, for the sake of simplicity, a follower motion restricted to a translation along the  $z$  axis is here considered, with a fixed attitude. The position  $z_f$ , velocity  $\dot{z}_f$  and acceleration  $\ddot{z}_f$  of the aircraft are submitted to a simplified 'spring-mass' system, with the aircraft mass  $M$ , and the prescribed stiffness and damping  $K_z$  and  $C_z$ . The last two coefficients are chosen in order to obtain a behavior crudely mimicking the time response of a full aircraft equipped with an autopilot. The other degrees of freedom (pitch, yaw, longitudinal and lateral motion) are frozen, thus still allowing the use of the yawing and rolling moments as measurement.

Finally, the equations of motion simplify to

$$M\ddot{z}_f + C_z\dot{z}_f + K_z z_f = -\frac{1}{2}\rho U_\infty^2 S C_L, \quad (7)$$

with  $C_L$  the lift coefficient computed using the aerodynamics model. Note that the same dynamics were imposed to the follower in the simulations presented in Section III.

For the second strategy with the flight dynamics model, the state vector is thus

$$\mathbf{q}_{\text{dyn}} = [\alpha_g, \Gamma_0, \Delta y, \Delta z, z_f, \dot{z}_f]^T, \quad (8)$$

and the kinematics variables turn readily into additional available measurements, thus leading to

$$\mathbf{m}_{\text{dyn}} = [\alpha_g, C_n, C_l, z_f, \dot{z}_f]^T. \quad (9)$$

For an actual aircraft, it is assumed that measurements of  $z_f$  and  $\dot{z}_f$  are available through a global navigation satellite system augmented with an inertial navigation system.

Due to the motion of the follower however, some adjustments are also necessary in the model for aerodynamics, in which steadiness was inherently assumed. First, the angle of attack is updated with

$$\alpha = \alpha_g - \frac{\dot{z}_f}{U_\infty}. \quad (10)$$

Besides, when the follower moves, the structure of its wake changes and therefore the circulation distribution too; this is not captured by the above aerodynamic model. To account for that effect, an approach similar to that proposed in [31] is adopted. Instead of dynamically computing the geometry of the shed vorticity evolving with the aircraft motion, the circulation distribution is decomposed in a steady part,  $\Gamma_{PLL}$ , resulting from the resolution of the Prandtl Lifting Lines (with a steady wake), and an unsteady part, assuming they can be added by superposition. The unsteady part must be evaluated by means of another method (analytical or numerical).

For this purpose, a dedicated numerical experiment is conducted to compute the indicial response of the circulation to a change in velocity. The simulation is performed using the same VPM method as presented in Section III, and the response of  $\Gamma$  to a unit step in  $\dot{z}_f$  is recorded. By computing the difference between this fully unsteady response and that obtained with the PLL model under the same conditions, one obtains  $\delta\Gamma_{d\dot{z}_f}(y, t)$ , the supplement which must be added to the PLL model in order to account for unsteadiness during a step in  $\dot{z}_f$ . In the end, the unsteady circulation distribution over the wing at iteration  $n$  for an arbitrary history of velocity is recovered from Duhamel's integral [32]

$$\Gamma(y, \mathbf{q}_n, \mathbf{q}_{n-1}, \mathbf{q}_{n-2}, \dots) = \Gamma_{PLL}(y, \mathbf{q}_n) + \sum_{k=0}^K \delta\Gamma_{d\dot{z}_f}(y, k \, dt) \dot{z}_f(n - k) dt. \quad (11)$$

## V. Results on steady wake

The efficiency of the EnKF is first demonstrated on a steady case, where the leader is trimmed and the follower is held at a fixed location with respect to the leader. This location is chosen so that the follower is close to the optimal position that should be flown to maximize the benefits of formation flight ( $\frac{\Delta y}{b} = 1.2, \frac{\Delta z}{b} = 0$ ). This setup is very similar to the static configurations considered in [14]. Yet, the steady state 3-D wake of the two aircraft (shown in Fig. 1a) is here obtained using a numerical simulation, and that the 'truth' measurements ( $\mathbf{z}$ ) are retrieved from that high-fidelity solution.

For the following example, the filter implements the first wake sensing strategy (Strategy 1), where the state vector is  $\mathbf{q} = \mathbf{q}_{\text{aero}}$ , and the measurements are limited to the geometric AoA and the circulation distribution samples:  $\mathbf{m} = [\alpha_g, \Gamma(y_1), \dots, \Gamma(y_9)]^T$ . The size of the ensemble is set to  $N = 50$  (as in the rest of this work). The filter (denoted from here on *filter IA*) is initialized with a starting guess away from the actual solution, and it is then advanced over 100 iterations.

As observed in Fig. 3, the convergence of the filter is obtained after 20 iterations, which is reasonably fast. A very good quality state estimate is obtained at convergence, as all the states remain within 10% error of their actual value.

In particular, the geometric AoA is very accurately reproduced (with a very small standard deviation), even though the standard deviation of the associated measurement noise was set to 5%. This reflects the fact that this state is directly measured, while it also has a great influence on the circulation measurements.

Advantageously, the use of  $\alpha_g$  in the state vector allows for a better prediction of the circulation of the vortices  $\Gamma_0$  (as compared to [14]). Indeed, it helps discriminate which part of the circulation measurements comes from the follower's flight attitude, and which part comes from the external influence of the leader's wake vortices.

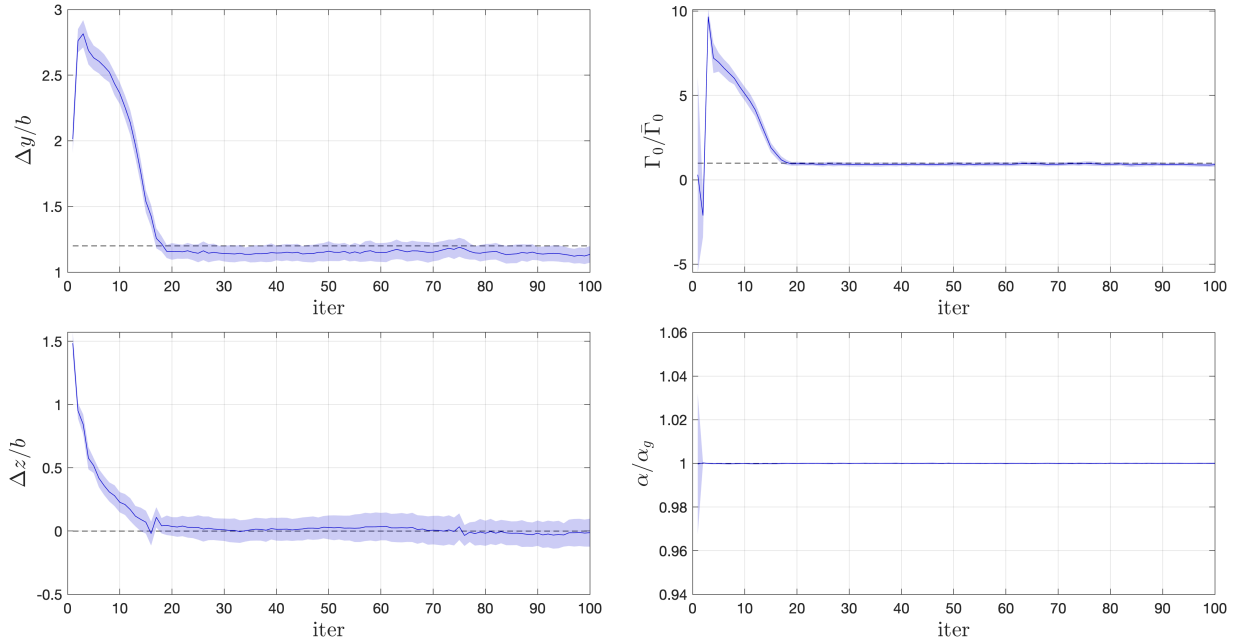


**Figure 3** Performance of the EnKF working on a steady wake, and actual value of the parameters (- -). The shaded areas show the  $1\text{-}\sigma$  confidence interval.  $\bar{\Gamma}_0$  is the average strength of the actual vortices.

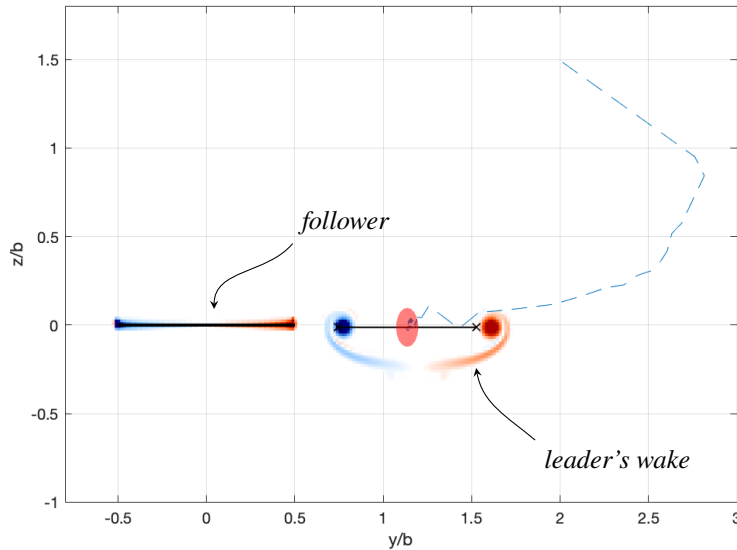


**Figure 4** Cross-section of the flow at  $x = 0$ , showing the vorticity from the numerical simulation and the estimated position of the leader's vortices ( $\times$ — $\times$ ) after 100 iterations of the EnKF, with an initial guessed position at  $(y = 2.0, z = 1.5)$ . The blue dashed line is the history of estimated position and the red shaded area represents the  $1\text{-}\sigma$  confidence interval on the estimated position of the center of the wake.

Noticeably, the estimated position of the wake center seems to be shifted to a smaller  $\Delta y$ . This is easily explained from the analysis of Fig. 4: the estimate is such that the predicted left-side vortex pinpoints the actual one. The latter is indeed having the greatest influence on the measurements. On the other hand, the value of  $b_0$  used in the surrogate model turns out to be slightly smaller than that of the actual wake, resulting in a small model error. Both factors explain

the deviation in terms of  $\Delta y$ , which would eventually have no consequence in formation flight, as the follower still correctly estimates the position of its closest neighbouring vortex.

The region of uncertainty associated with the estimated wake position is of the order of the size of the wake vortices cores. It can also be seen that the vortices are not fully rolled-up, as one can still distinguish traces of the vortex sheet shed by the wing of the leader.

It is worth mentioning that, among all the combinations of  $(\Delta y, \Delta z)$  and initial guesses tested in the frame of this work, none lead to the divergence of the filter. This is a clear argument to confirm that the sometimes divergent behaviors observed in [14] when using an Extended Kalman Filter on the same problem is due to the non-linearity of the problem. This non-linearity is here better handled with the EnKF.

## VI. Results on unsteady wake

As shown in [14] and [15], the observability of the process at hand is compromised in some configurations when the estimator only uses spanwise distributed measurements. This is due to the symmetry of the setup: the vertical velocity induced on the follower's wing by vortices located at different locations can be the same. For example, a vortex pair of given  $\Gamma_0$  and  $b_0$ , located at some  $(\Delta y, \Delta z)$  will produce the same circulation distribution on the follower as that obtained with the same pair of vortices located at  $(\Delta y, -\Delta z)$ .

Unsteadiness in the wake is known to improve the observability of the process, from the follower's perspective. This is investigated in the following example, where a sinusoidal heaving motion is prescribed to the leader aircraft, which thus oscillates around the equilibrium position used in Section V. This produces unsteady wake vortices apparently going up and down at the location of the follower. The dynamics of the latter is affected by the motion of the vortices, and its response is bound to Eq. (7).

### A. Strategy 1 based on circulation measurements

*Filter 1A* is tested on this unsteady case, along with a slightly modified version of it (*filter 1B*) having a measurement vector extended with the yawing moment measurement ( $\mathbf{m}_{1B} = [\alpha, \Gamma(y_1), \dots, \Gamma(y_9), C_n]^T$ ). The performances of the estimations by *filter 1A* and *filter 1B* are compared in Fig. 5.

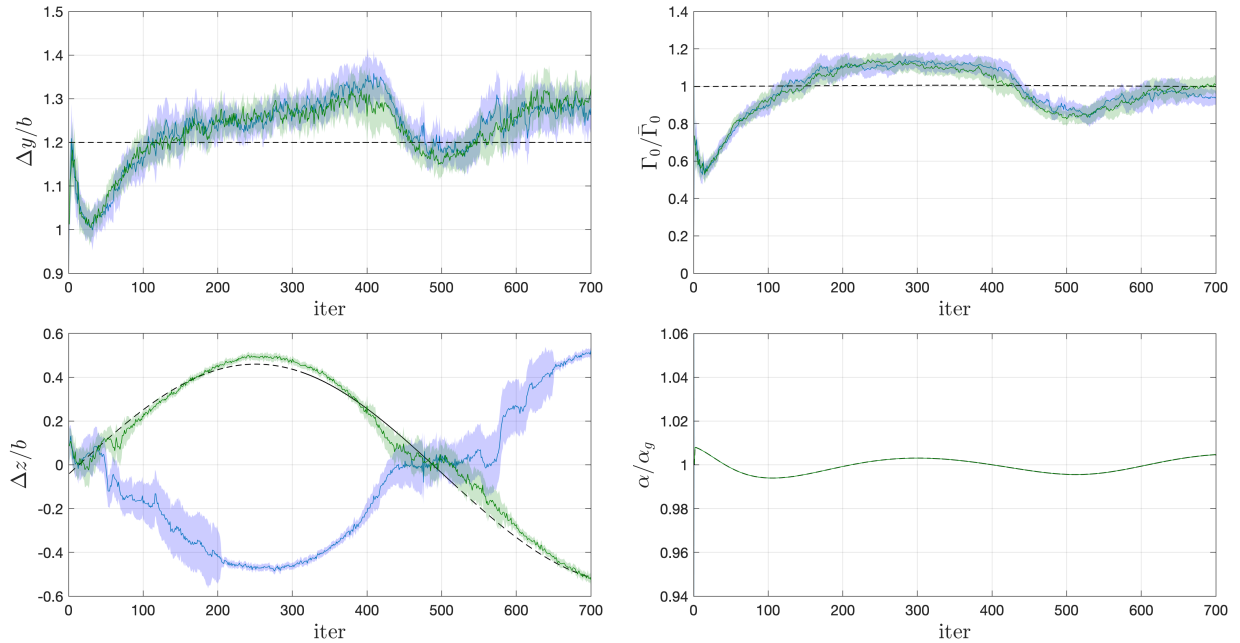


**Figure 5** Performance of the EnKF over time using Strategy 1: estimation using *filter 1A* (—), *filter 1B* (—), and actual value of the parameters (- -). The shaded areas show the 1- $\sigma$  confidence interval.

On the one hand, it is clear that *filter 1A* suffers from the previously exposed observability issue as the estimated

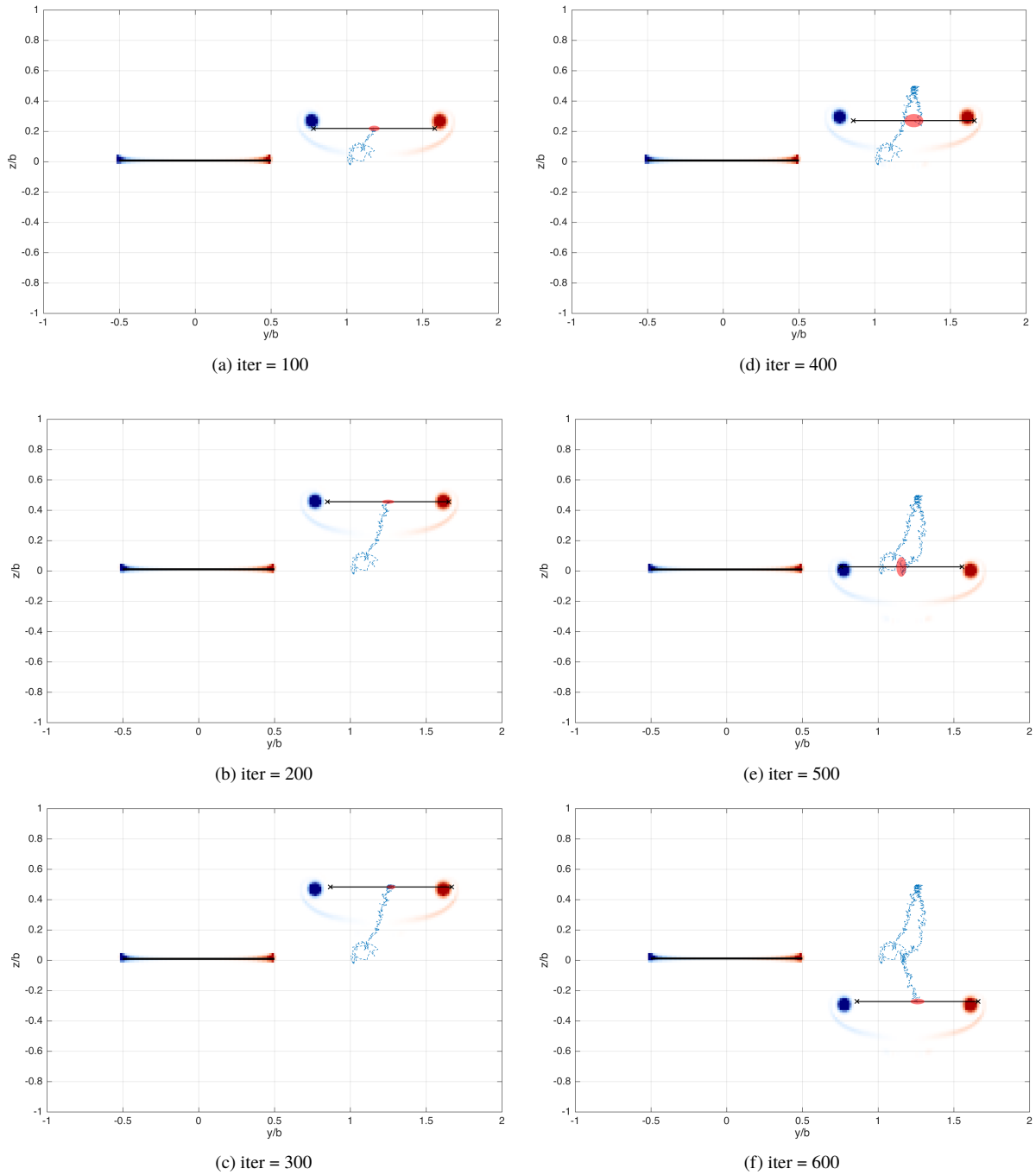


**Figure 6** Instantaneous cross-section ( $x = 0$ ) of the vortex system, and position of the wake estimated by the EnKF ( $\times$ — $\times$ ) at several iterations, using *filter 1B*. The blue dashed line is the history of estimated position and the red shaded area represents the  $1-\sigma$  confidence interval on the estimated position of the wake center.

$\Delta z$  appears to have a phase shifted from  $\pi/2$  with respect to the actual position of the vortices. There is not enough information in the measurements for the estimator to select the correct phase, in spite of the dither signal introduced in the leader's wake position.

On the other hand, *filter 1B* provides a good quality estimate of the position of the vortices, with a maximum error of about  $0.1b$  in  $y$  and  $z$ . Furthermore, this behavior was observed on several other test cases (not shown here): *filter 1B* was always able to lock onto the correct solution. This demonstrates that the yawing moment is well suited for breaking the symmetry in the problem: the velocity induced by the wake vortices on the VTP does not exhibit an up/down symmetry.

Incidentally, the dither in the wake position does have a beneficial effect as the standard deviation associated with the relative position of the wake is globally decreased with respect to the steady flight configuration. Notice that the standard deviation of  $\Delta z$  systematically increases when the value of the mean estimated value comes close to zero. Again, this is attributed to the symmetry of the problem: some ensemble members are spread around the actual solution, others around the symmetric one. Close to  $\Delta z = 0$ , the variations of  $C_n$  are too small to exclude the wrong solution. As a result, the ensemble distribution has two lobes, which virtually increases  $\sigma_{\Delta z}$ .

The AoA is again very accurately reproduced by both filters. The small amplitude oscillation comes from the follower's own motion (Eq. (10)).

When compared to the steady case, the estimation of  $\Gamma_0$  is of poorer quality: the quite large predicted oscillations are coupled to the variation of  $\Delta y$ . There is indeed an intrinsic correlation between these two quantities, as a strong wake located far away from the follower can have an effect on the measurements similar to that of a weak wake located

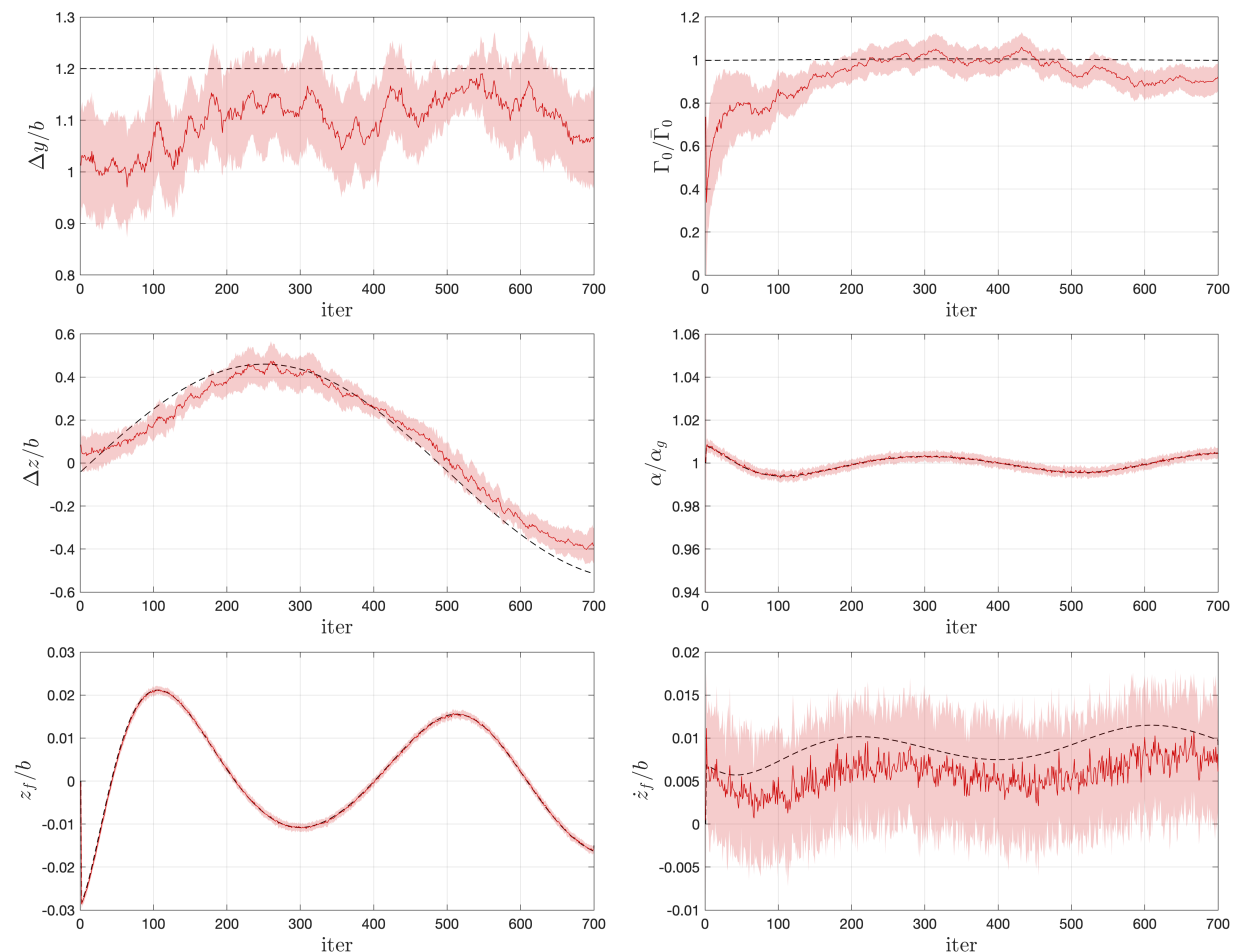


**Figure 7** Performance of the EnKF over time using Strategy 2: estimation (—) and actual value of the parameters (- -). The shaded areas show the  $1\text{-}\sigma$  confidence interval.

closer. This tradeoff again points to a lack of observability of the system as formulated here.

Figure 6 shows the estimated position of the vortices at different iterations of *filter 1B*, superimposed over the actual instantaneous vorticity field. The position of the closest neighboring vortex is again well reproduced by the estimator.

## B. Strategy 2 based on flight dynamics measurements

The second strategy takes advantage of the flight dynamics model and its ability to predict the kinematics of the aircraft. The underlying objective of this strategy is to remove the reliance of the estimator on the spanwise distributed measurements. The estimator (*filter 2*) thus uses  $\mathbf{q} = \mathbf{q}_{dyn}$  and  $\mathbf{m} = \mathbf{m}_{dyn}$ . Its performance is here investigated on the same case of wake vortices with vertical dither.

With this strategy, the local information about the flow which was previously provided by the circulation measurement is now lost. It is here replaced by ‘global’ information: the rolling moment coefficient, which is related to the asymmetry of the circulation distribution, and the evolution in time of  $\dot{z}_f$ , which is related to the integral of the circulation distribution (i.e. the lift).

Results obtained using *filter 2* are shown in Fig. 7. The estimation exhibits a performance similar to that observed when using *filter 1B*, in terms of position and strength of the wake vortices. This proves that the choice of the state variables and measurements was appropriate, and that the estimation of the wake properties is possible without dedicated probes.

The error on the mean estimated position roughly stays within 15% of  $b$ , but the level of uncertainty is noticeably increased with respect to those observed with Strategy 1. This can be partially attributed to a model error: the HTP is not accounted for in the PLL model while there is one in the simulation, leading to different values of  $C_L$  and, therefore, to an inconsistent value of  $\dot{z}_f$  (compared to that measured). On the other hand, the estimates of  $z_f$ ,  $\dot{z}_f$  and  $\alpha$  are of outstanding quality, again because these quantities are directly measured.

The time evolution of the estimated position is shown in Fig. 8 for a series of iterations of the filter. It can be seen that the estimated position of the closest neighboring vortex follows well the actual vortex.

## VII. Results on wake with turbulence

The performance of the estimators working on a wake with ambient turbulence is now investigated. Indeed, turbulence is a natural source of process noise, and the present case will provide insightful information about the robustness of the estimators.

The wake is generated using the same configuration for the leader and the follower as in the previous unsteady case. However, a turbulent velocity field is here introduced at the inflow of the numerical simulation. The turbulent velocity field is homogeneous and isotropic, and corresponds to a turbulence intensity of  $TI = 0.5\%$  for the VPM simulation.

The results of the estimation performed by *filter 1B* and *filter 2* are compared in Fig. 9. As it could have been expected, the results are much less satisfactory, yet both filters globally capture the actual evolution of the wake position. In particular, both estimated  $\Delta z$  reproduce the large scale oscillation originating in the vertical dither of the wake, with an instantaneous error of up to  $0.5b$ , but often for a short time. The lateral relative position  $\Delta y$  and the wake strength  $\Gamma_0$  are subject to much larger and longer excursions, respectively with deviations of up to  $b$  and  $\Gamma_0$ . The largest errors in  $\Delta y$  occur when the wake is ‘‘far’’ from the follower (i.e. when  $\frac{\Delta z}{b} \approx \pm 0.5$ ).

Noticeably, the standard deviations of all the states have increased with *filter 1B*, reflecting that the ambient turbulence also introduces measurement noise through the circulation probes. On the other hand, the standard deviations associated with the *filter 2* are much less affected: because all the degrees of freedom of the follower are frozen except the vertical translation, only a few of the estimator measurements reveal the presence of the noise. This could be overcome by replacing the simplified equation of motion considered for this example by a more complete set of equations.

For a more visual interpretation, Figs. 10 and 11 show instantaneous views of the flow in the cross-section  $x = 0$ . Even though the estimated position of the wake is not very accurate, it is always located in the vicinity of the actual wake vortices. In particular, in the context of formation flight, one would require the follower aircraft to fly at the optimal location in the wake, that is just next to the leader’s vortices. If the follower aircraft was directed to move to that estimated location using its estimated values, it would indeed move toward the actual location of the wake. One could then expect that, as the follower himself will start to move toward the leader’s wake, the quality of the estimation would gradually improve as it comes closer to the vortices, and thanks to the increase in observability provided by the relative motion.

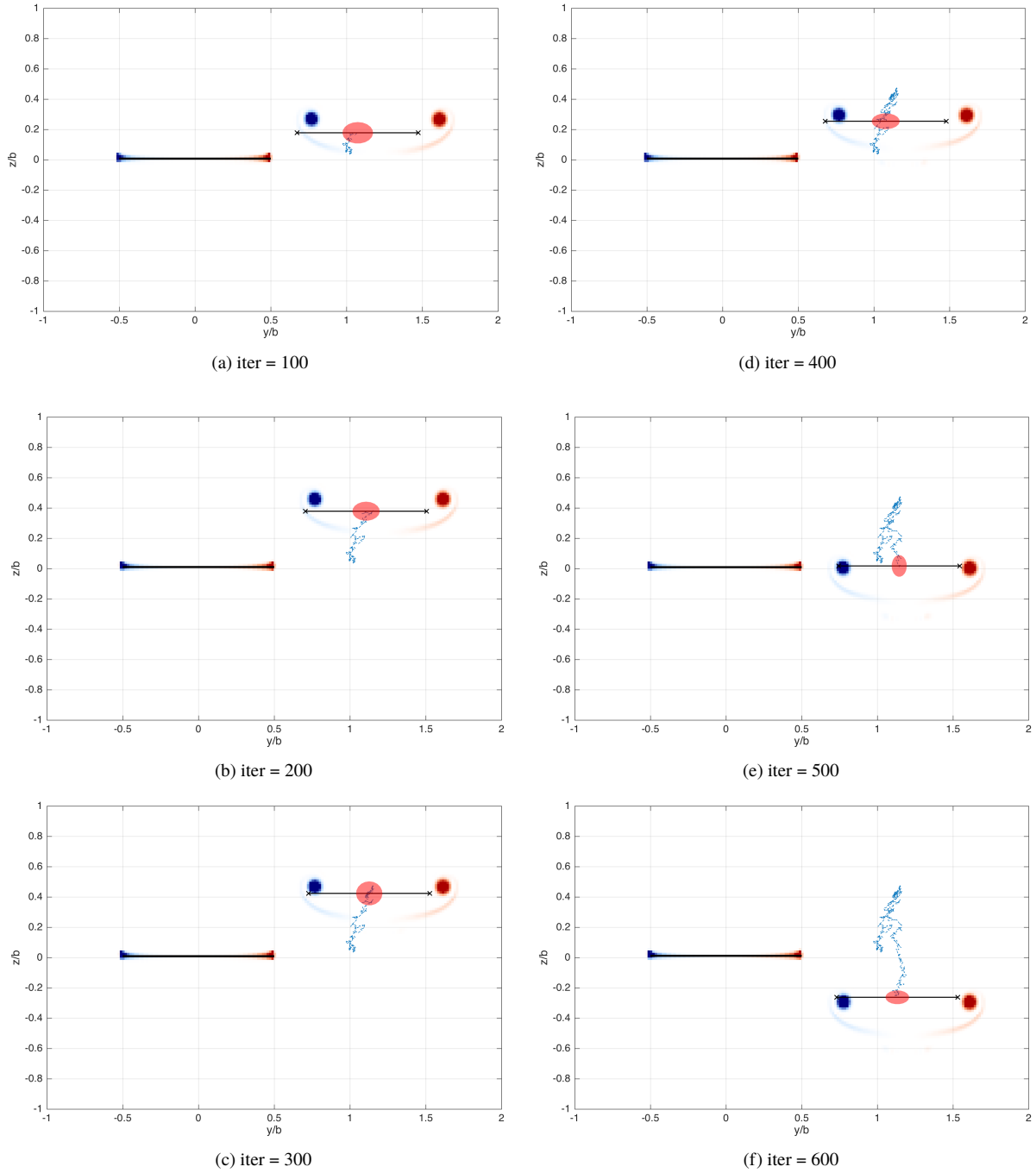


**Figure 8** Instantaneous cross-section ( $x = 0$ ) of the vortex system, and position of the wake estimated by the EnKF ( $\times$ — $\times$ ) at several iterations, using *filter 2* (Strategy 2).

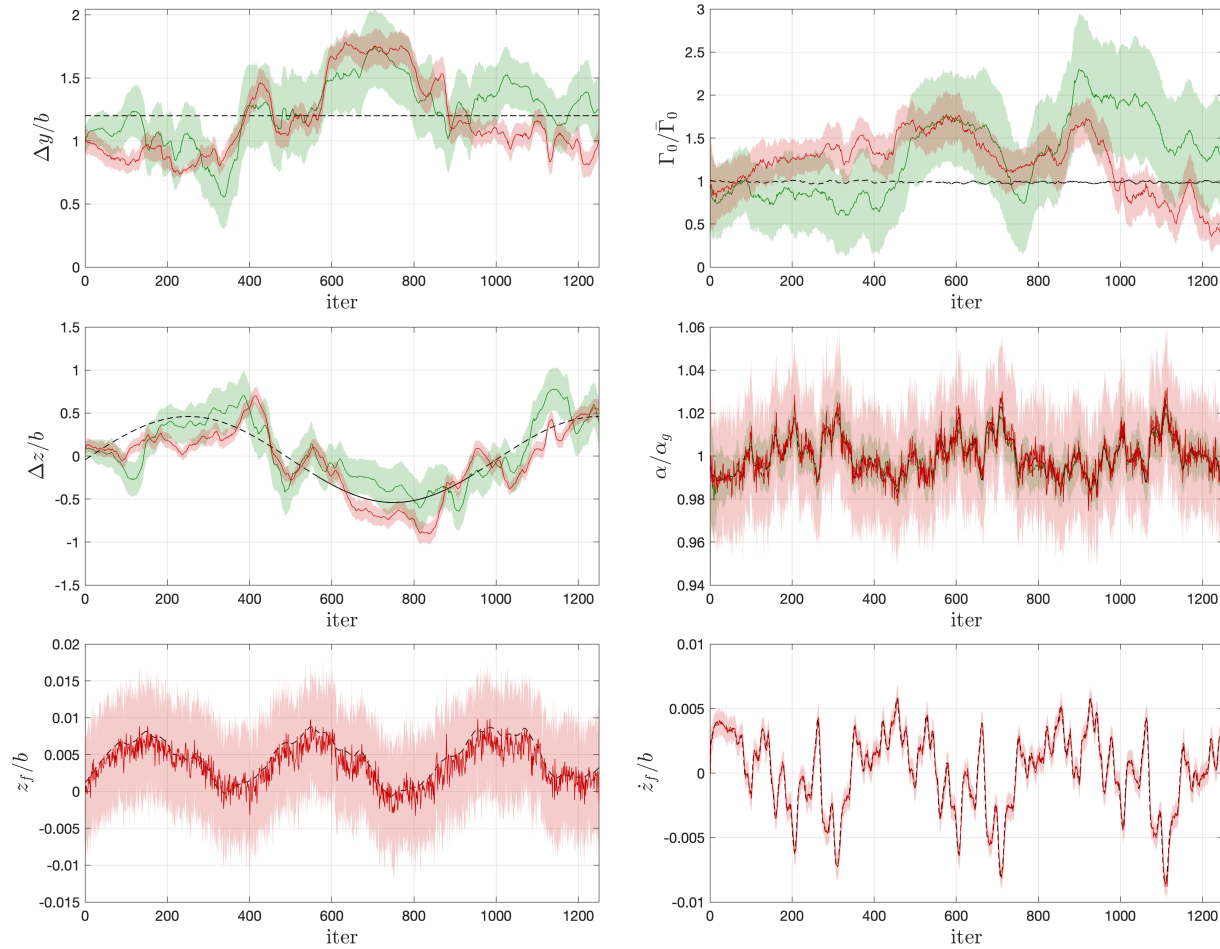


**Figure 9** Performance of the EnKF over time using *filter 1B* (—), *filter 2* (—) and actual value of the parameters (- -). The shaded areas show the 1- $\sigma$  confidence interval.

## VIII. Conclusions

This study investigated wake sensing techniques, towards the development of robust estimators for the detection and tracking of wake vortices in extended formation flight. The setup for these investigations consisted of a pair of aircraft flying in formation, with a leader producing wake vortices and with a follower trying to estimate its relative position with respect to those vortices. High fidelity reference data were obtained from the numerical simulation of the wake flow past the two aircraft using CFD. Three flight configurations were simulated in order to test the performances of the developed estimators under various conditions: one with a steady wake flow, one with an unsteady wake produced by a vertical heaving motion of the leader, and one where ambient turbulence was added to an unsteady wake. For each flight case, various measurements were extracted from the follower’s aerodynamics and vehicle dynamics in order to feed the estimators.

Two estimation strategies were studied, both exploiting the abilities of an Ensemble Kalman Filter (EnKF) to handle the non-linearity of the system. The first one used samples of the follower spanwise circulation distribution as a measurement, and the geometric angle of attack. It was shown that the addition of yawing moment to the measurements allowed to restore the observability of the process, otherwise hampered by an intrinsic symmetry in the formulation of the problem. In practice, this could be done equivalently with information coming from the rudder deflection.

The second strategy was designed so that the estimator does not require the spanwise distributed measurements. Instead, inputs from the flight dynamics and flight controls are used in the filter, in combination with a simplified model for the dynamics of the follower. The advantage of that approach is that it relies exclusively on data most likely already available aboard the aircraft (through flight computers and the flight control system).

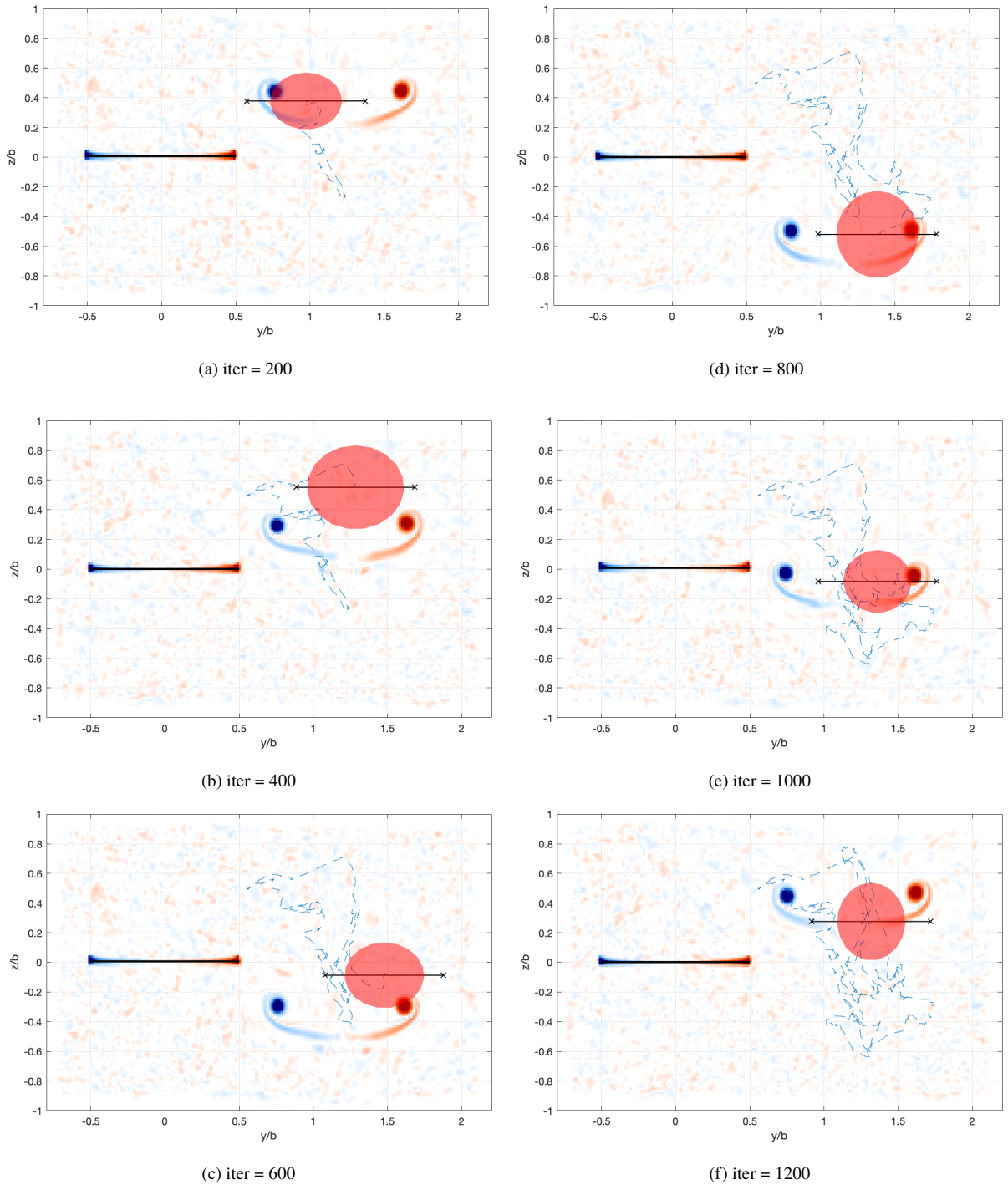


**Figure 10** Position of the vortex system estimated by the EnKF ( $\times$ — $\times$ ) at several iterations, using *filter 1B*, under noisy conditions due to ambient turbulence.

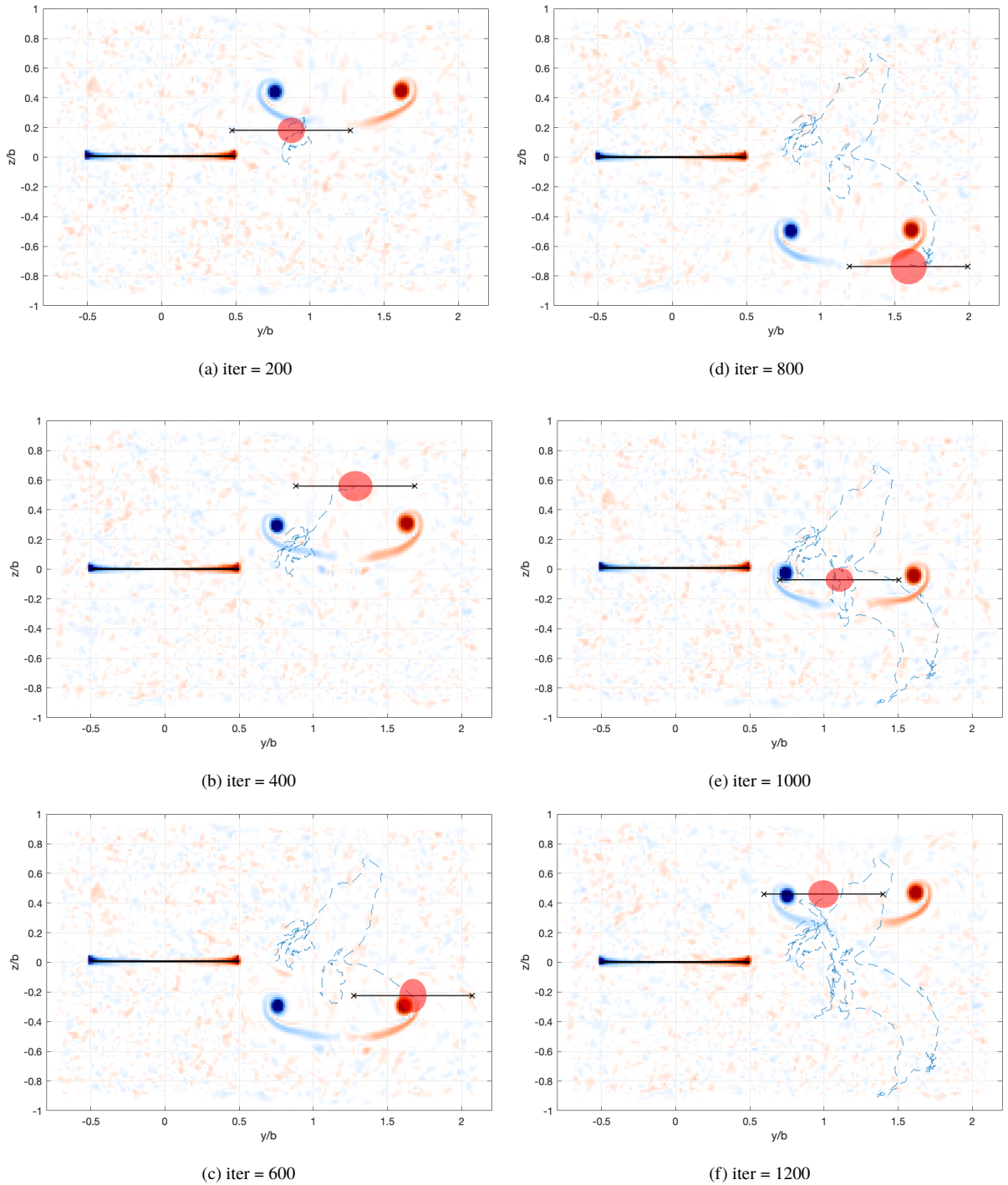


**Figure 11** Position of the vortex system estimated by the EnKF ( $\times$ — $\times$ ) at several iterations, using *filter 2*, under noisy conditions due to ambient turbulence.

Both strategies were proven successful at accurately tracking the position of the wake under various steady and unsteady flight conditions, showing that the EnKF performs better than the Extended Kalman Filter used in previous studies. Although not shown in this study, results obtained with the Unscented Kalman Filter also demonstrated an acceptable level of accuracy. Interestingly, the second strategy was almost as effective as the first one, even though a slightly increased error in the estimated position was observed. This demonstrates that the wake sensing can be performed by a follower aircraft without using costly dedicated sensors (e.g. retrofitted pressure probes along the wing).

Finally, the turbulent flight conditions were used to test the robustness of the estimators against noise. A clear loss of accuracy was observed in the estimations obtained from the two strategies. However, a better tuning of the parameters of the filters could lead to improved performances, while the second strategy could also benefit from relaxing the constraints that were here imposed on the follower's vehicle dynamics.

In future works, the wake sensing techniques will be enhanced to work with unconstrained follower aircraft dynamics. This will allow both strategies to be tested in a wider range of configurations, including more realistic cases such as dynamic ingresses of the follower into the wake of the leader. The estimator will also be used to provide the follower autopilot with the optimal location for maximizing the benefits of formation flight, in order to keep station with respect to that optimal relative positioning.

### Acknowledgments

The development work benefited from the computational resources provided by the supercomputing facilities of the Université catholique de Louvain (CISM/UCL) and the Consortium des Équipements de Calcul Intensif (CÉCI) en Fédération Wallonie Bruxelles (FWB) funded by the Fond de la Recherche Scientifique de Belgique (F.R.S.-FNRS) under Convention No. 2.5020.11.

### References

- [1] Hummel, D., "The use of aircraft wakes to achieve power reductions in formation flight," *AGARD FDP Symposium on 'The Characterization & Modification of Wakes from Lifting Vehicles in Fluid*, Vol. 36, DTIC Document, 1996, pp. 1–13.
- [2] Beukenberg, M., and Hummel, D., "Aerodynamics, performance and control of airplanes in formation flight," *ICAS, Congress, 17 th, Stockholm, Sweden, Proceedings.*, 1990, pp. 1777–1794.
- [3] Vachon, M., Ray, R., Walsh, K., and Ennix, K., "F/A-18 aircraft performance benefits measured during the autonomous formation flight project," Tech. Rep. TM-2003-210734, NASA, 2002. doi:10.2514/6.2002-4491.
- [4] Hanson, C. E., Pahle, J., Reynolds, J. R., and Andrade, S., "Experimental Measurements of Fuel Savings During Aircraft Wake Surfing," *2018 Atmospheric Flight Mechanics Conference*, 2018, p. 3560. doi:10.2514/6.2018-3560.
- [5] Vechtel, D., Fischenberg, D., and Schwithal, J., "Flight dynamics simulation of formation flight for energy saving using LES-generated wake flow fields," *CEAS Aeronautical Journal*, Vol. 9, No. 4, 2018, pp. 735–746. doi:10.1007/s13272-018-0318-z.
- [6] Ning, A., Flanzer, T. C., and Kroo, I. M., "Aerodynamic performance of extended formation flight," *Journal of Aircraft*, Vol. 48, No. 3, 2011, pp. 855–865. doi:10.2514/1.C031046.
- [7] Bieniawski, S. R., Rosenzweig, S., and Blake, W. B., "Summary of Flight Testing and Results for the Formation Flight for Aerodynamic Benefit Program," *52nd Aerospace Sciences Meeting*, AIAA, 2014, pp. 1–26. doi:10.2514/6.2014-1457.
- [8] Edstrand, A. M., Davis, T. B., Schmid, P. J., Taira, K., and Cattafesta, L. N., "On the mechanism of trailing vortex wandering," *Journal of Fluid Mechanics*, Vol. 801, 2016. doi:10.1017/jfm.2016.440.
- [9] Holzäpfel, F., "Effects of environmental and aircraft parameters on wake vortex behavior," *Journal of Aircraft*, Vol. 51, No. 5, 2014, pp. 1490–1500. doi:10.2514/1.C032366.
- [10] Daniels, T., Smith, W., and Kireev, S., "Recent developments on airborne forward looking interferometer for the detection of wake vortices," *4th AIAA Atmospheric and Space Environments Conference*, 2012, p. 2791. doi:10.2514/6.2012-2791.
- [11] Agnès, D.-B., Didier, G., Beatrice, A., Christophe, P., Didier, F., Laurent, L., Matthieu, V., and Claudine, B., "Onboard wake vortex tracking with an all fibered Coherent 1.5 $\mu$ m Doppler LIDAR for aircrafts in formation flight," *19th Coherent Laser Radar Conference*, 2018, pp. 146–149.
- [12] Hallock, J. N., and Holzäpfel, F., "A review of recent wake vortex research for increasing airport capacity," *Progress in Aerospace Sciences*, Vol. 98, 2018, pp. 27–36. doi:10.1016/j.paerosci.2018.03.003.

- [13] Steen, M., and Hecker, P., “Investigating the Potential Future Usage of Combined Airborne Wake Vortex Prediction Models and Measurement Sensors,” *2018 Atmospheric and Space Environments Conference*, 2018, p. 3022. doi:10.2514/6.2018-3022.
- [14] Hemati, M. S., Eldredge, J. D., and Speyer, J. L., “Wake Sensing for Aircraft Formation Flight,” *Journal of Guidance, Control, and Dynamics*, Vol. 37, No. 2, 2014, pp. 513–524. doi:10.2514/1.61114.
- [15] DeVries, L., and Paley, D. A., “Wake Sensing and Estimation for Control of Autonomous Aircraft in Formation Flight,” *Journal of Guidance, Control, and Dynamics*, 2015, pp. 1–10. doi:10.2514/1.G001138.
- [16] Van Leeuwen, P. J., “Comment on “Data assimilation using an ensemble Kalman filter technique”,” *Monthly Weather Review*, Vol. 127, No. 6, 1999, pp. 1374–1377. doi:10.1175/1520-0493(1999)127<1374:CODAUA>2.0.CO;2.
- [17] Evensen, G., “Sequential data assimilation with a nonlinear quasi-geostrophic model using Monte Carlo methods to forecast error statistics,” *Journal of Geophysical Research: Oceans*, Vol. 99, No. C5, 1994, pp. 10143–10162. doi:10.1029/94JC00572.
- [18] da Silva, A. F., and Colonius, T., “A Bias-aware EnKF Estimator for Aerodynamic Flows,” *2018 Fluid Dynamics Conference*, 2018, p. 3225. doi:10.2514/6.2018-3225.
- [19] Darakananda, D., Eldredge, J., da Silva, A., Colonius, T., and Williams, D. R., “EnKF-based Dynamic Estimation of Separated Flows with a Low-Order Vortex Model,” *2018 AIAA Aerospace Sciences Meeting*, 2018, p. 0811. doi:10.2514/6.2018-0811.
- [20] Whitaker, J. S., and Hamill, T. M., “Evaluating methods to account for system errors in ensemble data assimilation,” *Monthly Weather Review*, Vol. 140, No. 9, 2012, pp. 3078–3089. doi:10.1175/MWR-D-11-00276.1.
- [21] Evensen, G., *Data assimilation: the ensemble Kalman filter*, Springer Science & Business Media, 2009. doi:10.1007%2F978-3-642-03711-5.
- [22] Julier, S. J., and Uhlmann, J. K., “Unscented filtering and nonlinear estimation,” *Proceedings of the IEEE*, Vol. 92, No. 3, 2004, pp. 401–422. doi:10.1109/JPROC.2003.823141.
- [23] Backaert, S., Chatelain, P., and Winckelmans, G., “Vortex Particle-Mesh with Immersed Lifting Lines for Aerospace and Wind Engineering,” *Symposium on Particle Methods in Fluid Dynamics*, Procedia IUTAM, Vol. 18, edited by J. H. Walther, IUTAM, DTU Copenhagen, 2012, pp. 1–7. doi:10.1016/j.piutam.2015.11.001.
- [24] Chatelain, P., Curioni, A., Bergdorf, M., Rossinelli, D., Andreoni, W., and Koumoutsakos, P., “Billion vortex particle Direct Numerical Simulations of aircraft wakes,” *Computer Methods in Applied Mechanics and Engineering*, Vol. 197, No. 13, 2008, pp. 1296–1304. doi:10.1016/j.cma.2007.11.016.
- [25] Chatelain, P., Duponcheel, M., Caprace, D.-G., Marichal, Y., and Winckelmans, G., “Vortex particle-mesh simulations of vertical axis wind turbine flows: from the airfoil performance to the very far wake,” *Wind Energy Science*, Vol. 2, No. 1, 2017, p. 317. doi:10.5194/wes-2-317-2017.
- [26] Chatelain, P., Duponcheel, M., Zeoli, S., Buffin, S., Caprace, D.-G., Winckelmans, G., and Bricteux, L., “Investigation of the effect of inflow turbulence on vertical axis wind turbine wakes,” *Journal of Physics: Conference Series*, Vol. 854, No. 1, 2017, p. 012011. doi:10.1088/1742-6596/854/1/012011.
- [27] Caprace, D.-G., Buffin, S., Duponcheel, M., Chatelain, P., and Winckelmans, G., “Large Eddy Simulation of Advancing Rotor for Near to Far Wake Assessment,” *43rd European Rotorcraft Forum*, Milan, Italy, 2017, p. 570.
- [28] Jeanmart, H., and Winckelmans, G., “Investigation of eddy-viscosity models modified using discrete filters: A simplified regularized variational multiscale model and an enhanced field model,” *Physics of Fluids*, Vol. 19, No. 5, 2007, p. 055110. doi:10.1063/1.2728935.
- [29] Mann, J., “Wind field simulation,” *Probabilistic Engineering Mechanics*, Vol. 13, No. 4, 1998, pp. 269–282. doi:10.1016/S0266-8920(97)00036-2.
- [30] McCormick, B. W., *Aerodynamics, aeronautics, and flight mechanics*, John Wiley, 1995.
- [31] Drela, M., “Integrated simulation model for preliminary aerodynamic, structural, and control-law design of aircraft,” *AIAA Paper*, Vol. 99, 1999, p. 1394. doi:10.2514/6.1999-1394.
- [32] McRuer, D. T., Graham, D., and Ashkenas, I., *Aircraft dynamics and automatic control*, Vol. 740, Princeton University Press, 2014.